Modeling of plasma jet of vacuum arc with copper-chromium cathode under action of strong axial magnetic field

Journal of Physics: Conference Series **1393** (2019) 012025 doi:10.1088/1742-6596/1393/1/012025

Modeling of plasma jet of vacuum arc with copper-chromium cathode under action of strong axial magnetic field

D L Shmelev[1,2], **I V Uimanov**[1] **and V P Frolova**[3]

[1] Institute of Electrophysics UD RAS, 106 Amundsen Str., Yekaterinburg, 620016, Russia
[2] Ural Federal University, 19 Mira Str., Ekaterinburg, 620002, Russia
[3] Institute of High Current Electronics SB RAS, 2/3 Academichesky Ave., Tomsk, 634055, Russia

E-mail: shmelev@iep.uran.ru

Abstract. This paper deals with the computer simulation of a vacuum arc with composite cathode under action of external axial magnetic using hybrid model. The described hybrid model treats the electrons as a massless fluid and ions as macroparticles. It is shown that the average charge state of ions in a jet of a vacuum arc increases with increasing magnetic field. The calculation results are consistent with experimental data.

1. Introduction

High-current vacuum arcs (HCVA) arising in vacuum interrupters with an axial magnetic field (AMF) can operate in different modes [1, 2]. When AMF is higher than about of 10 $mT \cdot kA^{-1}$, HCVA exhibits a multiple arc mode. In this mode HCVA looks like a lot of low current vacuum arcs (LCVA) working in parallel. Therefore, it is of great practical interest to study the characteristics of a single spot with the corresponding plasma jet in a strong AMF as part of the HCVA in vacuum interrupters. LCVA (current – several tens amperes) in various magnetic field for short gap distances (2–8 mm) were studied experimentally [3–5]. However, the study focused mainly on the optical characteristics of the plasma. The effect of AMF on the ion average charge state (ACS) in a LCVA plasma jet was investigated in [6].

Another practical interest associated with vacuum interrupters is a vacuum arc with composite electrodes. Nowadays, electrodes from a copper-chromium composite are most widely used in interrupters. Recently, the influence of AMF on ion ACS in vacuum arc plasma jet with composite copper-chromium cathode was investigated [7]. It was shown that an increasing the AMF increases the charge state of copper and chromium ions in the composite cathodes like in single-element cathodes, and as the magnetic field is increased to more than 0.8 T, the increase in the charge state slows down.

In the paper a computer simulation is used to model the influence of the AMF on ion ACS in plasma jet of a low current vacuum arc burning on a composite cathode. Hybrid model [8, 9] is used for the simulation. The hybrid model describes the electron subsystem as a massless liquid with the help of MHD method, but describes ions as particulates using the particle-in-cell (PIC) method.

2. Model description

The described model is an axisymmetric 2D hybrid model, similar to that used in [9]. This model differs from model [9] using two different types of atoms and ions: copper and chromium.

The motion of ions and neutrals are described with the help of particle-in-cell (PIC) approach:

$$\frac{d\vec{r}_i}{dt}=\vec{V}_i,\ m_i\frac{d\vec{V}_i}{dt}=e_iE+\frac{e_i}{c}\vec{V}_i\times\vec{B}+\left(\frac{\delta m_i\vec{V}_i}{\delta t}\right)_{ii}+\left(\frac{\delta m_i\vec{V}_i}{\delta t}\right)_{ie}, \tag{1}$$

$$\vec{E}=-\frac{\vec{\nabla}P_e}{en_e}-\frac{1}{c}\vec{u}_e\times\vec{B}-\frac{1}{en_e}\left(\frac{\delta m_e\vec{V}_e}{\delta t}\right), \tag{2}$$

$$n_i=\frac{1}{H_c}\sum_{k=1}^{N_c}S(\Delta x_k),\ \vec{u}_i=\frac{1}{H_c}\sum_{k=1}^{N_c}\vec{V}_kS(\Delta x_k),\ T_i=\frac{1}{H_c}\sum_{k=1}^{N_c}\frac{m_i}{3}\left(\vec{V}_k-\vec{u}_i\right)^2S(\Delta x_k), \tag{3}$$

where V_i – velocity of ion (of type i) macroparticles, r_i – ion macroparticles radius vector, S – shape function of macroparticle (bilinear interpolation was used), H_c – form factor of cell, N_c – number of macroparticles in cell, n_i – ion density, n_e – electron density, u_i – ion drift velocity, τ_{ei} – electron-ion collision time, B – magnetic field, E – electric field, P_e – electron pressure. The last two terms at the right-hand side of the second equation (1) denotes the momentum change due to ion-ion and ion-electron coulomb collisions, which considered with the help of MC method. Last term in (2) denotes the averaged electron momentum change in electron-ion coulomb collisions. Electron subsystem is treated as massless fluid with quasineutrality assumed:

$$n_e=\frac{1}{e}\sum_i e_in_i,\ \vec{u}_e=\frac{1}{en_e}\left(\sum_i e_in_i\vec{u}_i-\vec{J}\right), \tag{4}$$

$$\frac{3}{2}n_e\left(\frac{\partial T_e}{\partial t}+\vec{u}_e\nabla T_e\right)+P_e\vec{\nabla}\cdot\vec{u}_e+\vec{\nabla}\chi\vec{\nabla}T_e=\left(\frac{1}{2}\frac{\delta m_e\left(\vec{V}_e-\vec{u}_e\right)^2}{\delta t}\right)-W_r-W_{ion}, \tag{5}$$

where J – total arc current density, u_e – the electron drift velocity, λ – plasma thermal conductivity, W_r – radiative losses, W_r – loss energy for ionization. First term at right-hand side of (5) denotes the averaged electron chaotic energy change due to electron-ion coulomb collisions. Electromagnetic equations for 2D cylindrical geometry are reduced to the equation for θ-component of magnetic field:

$$\frac{\partial B_\theta}{\partial t}+\frac{\partial u_{ez}B_\theta}{\partial z}+\frac{\partial u_{er}B_\theta}{\partial r}-\frac{\partial u_{e\theta}B_z}{\partial z}=\frac{c^2}{4\pi}\left(\frac{\partial}{\partial r}\left(\frac{1}{r\sigma}\frac{\partial rB_\theta}{\partial r}\right)+\frac{\partial}{\partial z}\left(\frac{1}{\sigma}\frac{\partial B_\theta}{\partial z}\right)\right) \tag{6}$$

Because of relatively low current in described vacuum jet, the axial magnetic field is assumed to be constant B_z. Then the components of current density are:

$$J_\theta=\omega_c\,\tau_{ei}\left(J_r-\sum e_in_iu_{ir}\right),\ J_z=\frac{c}{4\pi}\frac{1}{r}\frac{\partial rB_\theta}{\partial z},\ J_r=-\frac{c}{4\pi}\frac{\partial B_\theta}{\partial z}. \tag{7}$$

where σ – plasma (Spitzer) conductivity, ω_c – electron cyclotron frequency.

Ions undergo ion-ion and electron-ion Coulomb collisions. To perform electron-ion collisions a temporarily electron subsystem is generated at every step. This system is modeled by shifted Maxwell distribution. Grid values for T_e, n_e and u_e are used as the moments to generate the distribution function. The collisions are taken into account by using the DSMC-like method [9].

The losses of energy for ionization W_{ion} in (5) were calculated in the course of simulation of ionization and recombination reactions. The reactions were simulated with the help of direct simulation Monte Carlo method (DSMC) [10] with the use of zero collision technique to speed up the calculations. Direct ionization, triple recombination, photorecombination were taken into account. Briefly, the key idea of the method was to firstly estimate the maximum possible number of the collisions:

$$N_r = z\, N_c^2 w \beta\left(T_e\right)_{\max} \frac{dt}{H_c}, \tag{8}$$

where z – average ionization state of ions in the cell, w – statistical weight of the particles in the cell, β_{max} – maximum of reaction rate coefficient. When the N_r particles are chosen randomly, then we can estimate the statistical weight and the total reaction rate for a given particle. If the random number $R < (\beta_k/\beta_{max})$ then the reaction with the given particle had taken place, if not – the zero collision had occurred. Thus, the actual number of reactions is normally much less than N_r. Then the specific type of collision can be chosen randomly (in proportion to the specific reaction rate). After that, the particle type should be modified accordingly and W_{ion} can be calculated.

Cathode boundary conditions mimic the cathode group spot. A number of small areas at the cathode emit current and ion flux in a cone with the angle of $\pi/2$. The surface between the cells is inactive one. In the present calculations the simplest two-cell arrangement is used. Actually the cell 1 has a circle shape but the cell 2 has a ring shape (because of axial symmetry). Radius of the cathode grope spot in the simulation is 100 μm. It is assumed that the current per group spot is 60 A.

The parameters of plasma emitted by the spot are the following: ions velocity $V_i = 10^6$ cm·s^{-1}, electron temperature $T_e = 3$ eV, ion temperature $T_i = 0.5$ eV, specific ion erosion – 40 μg·C^{-1}. It is assumed that the plasma composition delivered by the cells is the same as the cathode composition. The compositions of the initial charge states for copper and for chromium are taken from [7] for the case without AMF. For copper the initial composition is 36% of Cu^{+1}, 52% of Cu^{+2}, and 12% of Cu^{+3}. For chromium the initial composition is 30% of Cr^{+1}, 59% of Cr^{+2}, and 11% of Cr^{+3}. These spot plasma parameters and the spot position are fixed during the calculations.

Calculation was made for the interelectrode gap distance – 0.4 cm, which corresponds to that used in experiment [7]. According to [8], the radius of the calculation domain per one group spot is estimated to be 1.3 cm. In HCVA, the group spot is usually surrounded by other cathode spots. To take this into account, the lateral boundary of the computational domain reflects all the falling ions and atoms. On the surface of the cathode surrounding the group spot, the generation of secondary plasma by sputtering and partial reflection of ions is taken into account (as in [9]). Where this is not specifically stated, the anode is the ideal collector.

3. Results and discussion

Under the action of an external strong AMP, a narrow jet is formed from plasma emitted by the group spot (figures 1–2). As expected, in calculations, the stronger the external AMF, the thinner the plasma jet. The dependences of some plasma parameters along the jet axis for different AMF are shown in figures 3–4. It is seen that on the way from the cathode to the anode, the ion density decreases from about of 10^{16} cm^{-3} to 10^{15} cm^{-3}. It is necessary to explain that the density 10^{16} cm^{-3} is not the real density in the cathode spot. This is an averaged density at a distance of hundred micrometers from the cathode spot. As it can be seen, ion density near the axis increases with increasing AMF. Obviously, this is caused by the compression of the plasma jet by applied AMF. The self-magnetic field of such a jet is too small to provide appreciable compression. As it can be seen in the cantor-plot (figure 1, right side), the lines of the constant densities at high AMF are approximately resembles the lines of the constant current densities (figure 1, left side), that is caused by the effective dependence of electric conductivity on the electron density in magnetized plasma due to Hall effect.

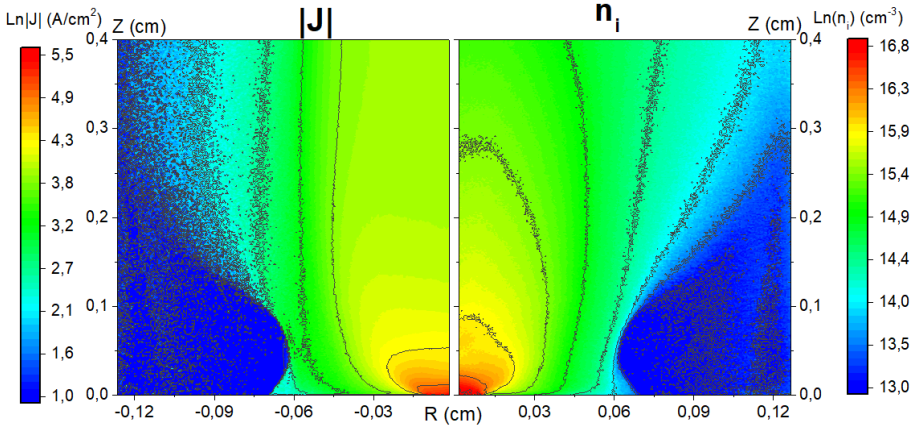

Figure 1. Current density distribution (left side), ion density distribution (right side). Cathode is at the bottom. Cathode – CuCr50; current 60 A; AMF – 1.2 T.

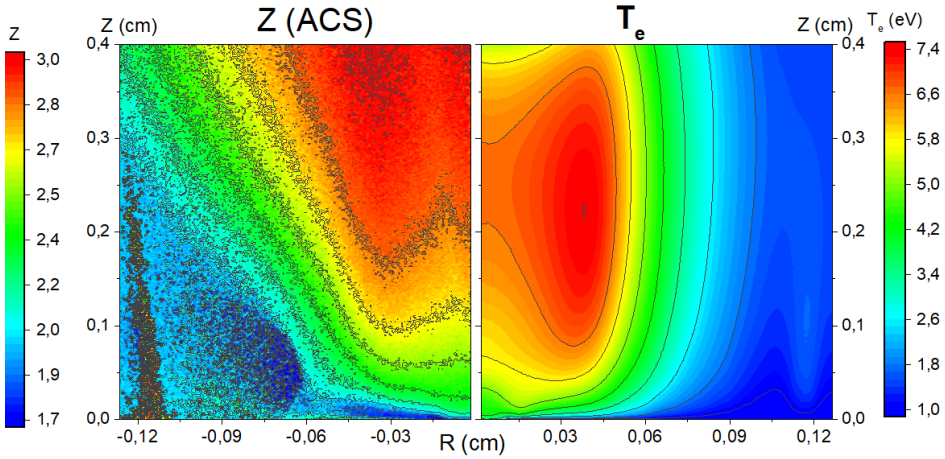

Figure 2. Distribution of ion ACS (left side), electron temperature distribution (right side). Cathode is at the bottom. Cathode – CuCr50; current 60 A; AMF – 1.2 T.

The behavior of electron temperature (T_e) in the gap can be seen in figure 4. The electron temperature in the middle of the gap increases with an increase in AMF because of the current channel constriction and the following increase in the current density. The electron temperature decreases in front of the anode because of cooling due to emission from plasma to the anode. The simultaneous increase in plasma density and electron temperature with increasing magnetic field leads to the expected increase in ion ACS (Z in figure 4). It is seen that a sharp increase in Z occurs near the spot. In addition, a gradual increase in Z occurs along the entire length of the jet.

Distributions on the anode of ions of different types along the radius are shown in figure 5. The masses of copper and chromium ions are quite close therefore the radial distribution of ions of different elements is similar. In the hypothetical composite CuC50 (figure 6), where one of the components (carbon) is much lighter than copper, the radial distributions of the components are very different from each other. Carbon has a much narrower radial distribution, since light ions are more strongly deflected by the magnetic field, and the plasma jet ion density is so low that ion-ion interaction unable to equalize the ion velocities. Recall that in the absence of AMF in arcs on composite cathodes, the situation is the opposite: light ions have a wider angular distribution than heavy ones [11, 12].

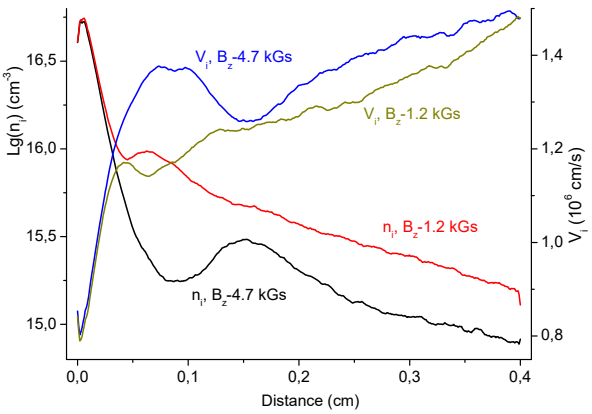

Figure 3. Ion density and ion drift velocity along the axis for different AMF. Cathode – CuCr50.

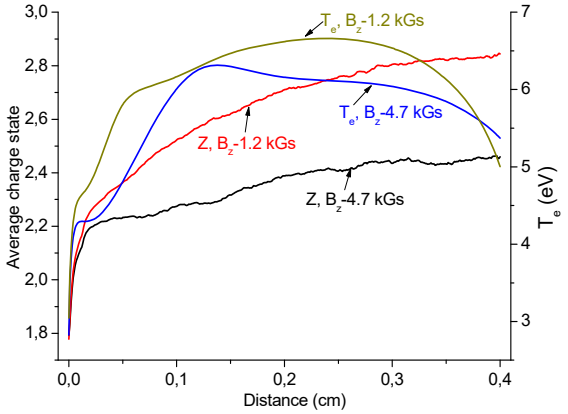

Figure 4. Ion average charge state and electron temperature along the axis for different AMF. Cathode – CuCr50.

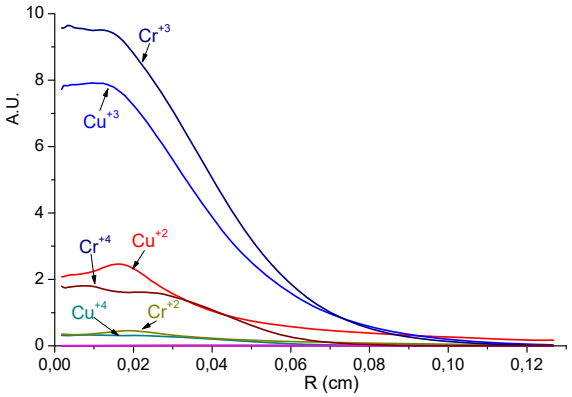

Figure 5. Radial distribution of different ion species on anode side. Cathode – CuCr50.

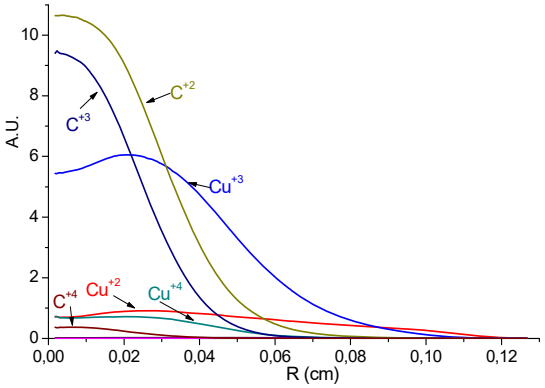

Figure 6. Radial distribution of different ion species on anode side. Cathode – CuC50.

The comparison of calculated ion ACS with experimental ones for different composite cathode is shown in figure 7. It can be seen that in both cases the ACS of copper and chromium ions increases with an increase in AMF. Moreover, at AMF from 0.4 to about 0.95 T, the rate of increase in ion ACS in the calculations is in good agreement with experiment. At AMF higher than 0.9 T, in the experiment, there is a decrease in ion ACS which is not in the calculations. In the experiment [7], this decrease is accompanied by a sharp increase in the fraction of singly charged ions. We believe that in this case, strong evaporation begins from the cathode and the anode grid elements. An illustrative calculation in which anode sputtering was supposed (as in [9]) showed a significant decrease in ion ACS (figure 7, cn-30).

Comparing the calculations and the experiment (figure 7), one can see that the calculation overestimates the chromium ions ACS. In experiments, there is always a very large percentage of singly charged ions. If we remove the singly charged component from the experimental results, the agreement with the calculation will significantly improve (figure 7, ec-30). This, in our opinion, indicates that, in addition to the purely ionic erosion, characteristic of spots of the second kind, substantial evaporation from the surface of the cathode near the cathode cells occurs in group cathode spots. This is particularly pronounced in the HCVA.

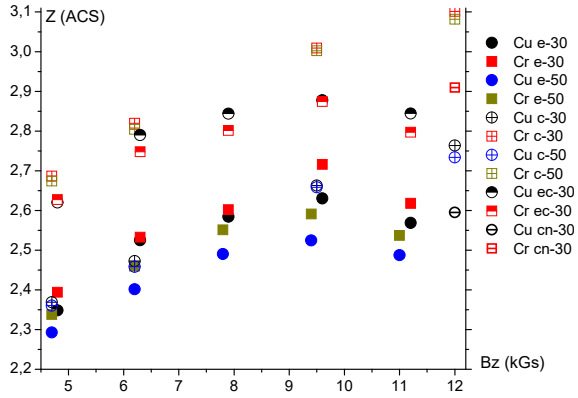

Figure 7. Comparison of calculated Cu-ion and Cr-ion ACS with experimental ones. Denotes: e-30 – CuCr30 experiment; c-50 – CuCr50 calculation; ec-30 – CuCr30 experiment singly charged ions is not included; cn-30 – CuCr50 calculation with anode sputtering.

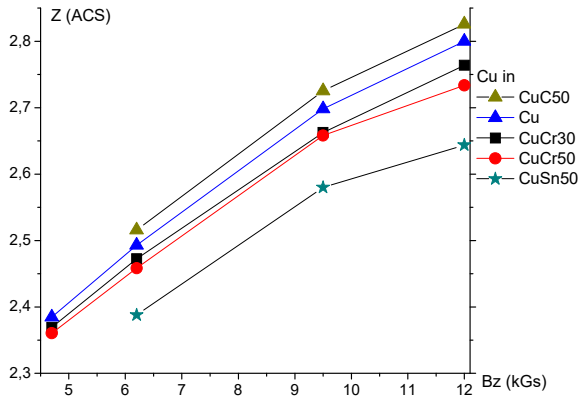

Figure 8. Dependence of Cu-ion ACS on AMF for arc with different composite cathode (calculation results).

The ACS of copper ions calculated for different composite electrodes is shown in figure 8. Comparing copper ion ACS in arc with electrodes made from Cu, CuCr30 and CuCr50 one can note that the more chromium admixture, the less the copper ion ACS. This dependence is present in the experiment [7], where it is much more pronounced. Recall that the ionization potentials of chromium are somewhat less than that of copper. In the calculations, the addition of chromium, this ultimately leads to a decrease in the electron temperature in the jet and, as a consequence, to a decrease in the ACS of copper ions. Figure 8 also shows the copper ion ACS in vacuum arcs with two hypothetical compositions CuSn50 and CuC50. In the first case, the tin component has ionization potentials considerably less than those of chromium and copper, therefore the copper ion ACS is less then in the case of CuCr50 cathode. In the second case, the carbon ionization potentials considerably higher than those of chromium and copper, therefore copper ion ACS is higher then in the case of CuCr50 cathode. Thus, in the case of a vacuum arc with strong AMF, the addition of a material with an ionization potential smaller than that of the main component to the composite cathode should lead to a decrease in the ACS of the ions of the main component (and vise versa). Recall that in the case of absence of the strong AMF this dependence is opposite one [13].

Acknowledgments
This work was supported by Russian Science Foundation (project No. 18-19-00069).

References

[1] Schade E 2005 *IEEE Trans. Plasma Sci.* **33** 384
[2] Slade P G 2008 *The vacuum Interrunter: theory, design and application* (CRC Press)
[3] Chaly A M, Logatchev A A, Taktarov R, Zabello K K and Shkol`nik S M 2009 *IEEE Trans. Plasma Sci.* **37** 1426
[4] Zabello K K, Logatchev A A, Taktarov R A and Shkol`nik S M, 2011 *IEEE Trans. Plasma Sci.* **39** 1319
[5] Wang C, Shi Z, Wu B, Gao Z, Jia S and Wang L 2016 *J. Phys. D: Appl. Phys.* **49** 135203
[6] Oks E M, Brown I G, Dickinson M R, MacGill R A, Emig H, Spädtke P and Wolf B H 1995 *Appl. Phys. Lett.* **67** 200
[7] Frolova V, Nikolaev A, Yushkov G and Oks E 2018 *Proc. 20th International Symposium on High-Current Electronics* (Tomsk, Russia) 214

[8] Shmelev D L and Uimanov I V 2015 *IEEE Trans. Plasma Sci.* **43** 2261
[9] Shmelev D L, Uimanov V I and Wang L 2017 *Proc. 4th International Conference on Electric Power Equipment- Switching Technology* (Xi'an; China) 642
[10] Serikov VV, Kawamoto S and Nambu K 1999 *IEEE Trans. Plasma Sci.* **27** 1389
[11] Nikolaev A G, Oks E M, Savkin KP, Yushkov G Yu, Frolova V P and Barengolts S A 2014 *J. Appl. Phys.* **116** 213303
[12] Shmelev D L, Barengolts S A, Uimanov I V, Tsventoukh M M and K.P. Savkin 2015 *J. Physics: Conf. Series* **652** 012041
[13] Shmelev D L, Barengolts S A and Savkin K P 2015 *Tech. Phys. Lett.* **41** 500